Limited Influence of Externally Introduced Pressure on the Hydrothermal Synthesis of $V_{1-x}W_xO_2$ (M)

Xinyu Guo[a], Dharmjeet Madhav[a], Hans Hallez[b], and Veerle Vandeginste[a]*

[a] Department of Materials Engineering, Surface and Interface Engineered Materials, Spoorwegstraat 12, 8200 Bruges, Belgium

[[b] Department of Computer Science, Mechatronics Research Group, Spoorwegstraat 12, 8200 Bruges, Belgium

* Corresponding Author: Veerle Vandeginste; E-mail: veerle.vandeginste@kuleuven.be

Abstract: Tungsten (W)-doped monoclinic vanadium dioxide ($V_{1-x}W_xO_2$ (M)) exhibits a reversible first-order metal-to-insulator transition within the temperature range of 20-50 ºC, with the atomic percentage of W (x) from 2.0 to 0.5 at%, making it a promising thermochromic material for energy-saving applications. However, preparing high-purity thermochromic $V_{1-x}W_xO_2$ (M) phase via a large-scale and cost-effective synthesis method remains a challenge due to the multiple polymorphs of VO_2 and its high sensitivity to synthetic parameters including temperature, time, and molar ratio of precursors. Here, we investigate the influence of externally introduced pressure on the hydrothermal synthesis of $V_{0.98}W_{0.02}O_2$ (M) by varying the pressure through the introduction of different amounts of either nitrogen or carbon dioxide gas into the system. These synthesized samples were characterized using X-ray diffraction, differential scanning calorimetry, and scanning electron microscopy. Results indicate that externally introduced pressure has no direct

significant effect on the formation of the $V_{0.98}W_{0.02}O_2$ (M) phase under our synthesis conditions, whereas it may affect the transformation of $V_{0.98}W_{0.02}O_2$ (M) by affecting the dissolution of CO_2 in water and then the H^+ content of the solution. In contrast, $V_{0.98}W_{0.02}O_2$ (M) formation is highly susceptible to temperature, with even a small variation (<5 °C) leading to significant differences in the reaction product composition. These findings unveiled that controlling temperature precisely is crucial for synthesizing $V_{1-x}W_xO_2$ (M) while externally introduced pressure plays a relatively negligible role, providing a reference for the high-efficiency and scalable synthesis of $V_{1-x}W_xO_2$ (M), and further promoting its application in smart windows, automotive glazing, and other energy-efficient technologies.

Keywords: vanadium dioxide, hydrothermal, synthesis parameters, energy materials, interfacial engineering

1. Introduction

Vanadium dioxide (VO_2) is a compound that occurs as multiple polymorphs, including VO_2 (A), VO_2 (B), VO_2 (D), VO_2 (M), VO_2 (R), and VO_2 (C) [1-3]. Among these, VO_2 (B) is recognized as a promising electrode material for lithium-ion batteries, exhibiting a reversible structural switch between crystalline and amorphous phases under high pressure [4-7]. VO_2 (A) is a metastable phase in the conversion process of VO_2 (B) to VO_2 (M) or VO_2 (R) [8]. The recently identified VO_2 (D) has been described by Wang et al. [9] as an oxygen-deficient variant of the VO_2 (M) phase [10]. Only VO_2 (M) and VO_2 (R) are known for their thermochromic properties, characterized by a metal-insulator phase transition at approximately 68 °C (T_c). This transition is accompanied by a reversible change in optical

property, from high infrared transmittance (insulating monoclinic, VO_2 (M)) at low temperature to high infrared reflectance (metallic tetragonal, VO_2 (R)) at high temperature [11-15]. Due to their thermochromic property, VO_2 (M/R) has attracted great interest for many promising applications in diverse fields, such as optical switching devices [16], gas and temperature sensors [17, 18], and smart windows [19, 20].

The synthesis of high-purity VO_2 (M) is critically dependent on the method employed. Several methods, including hydrothermal synthesis, sol-gel processes, and combustion techniques, have been developed to produce micro- or nano- VO_2 (M) with rhombohedral, rod-like or snowflake shapes [21-25]. Post-annealing treatments are often used to transform initial products (mainly VO_2 (B) or VO_2 (D)) into VO_2 (M) phase [26]. Among these methods, hydrothermal synthesis stands out due to its effectiveness in fabricating high-quality micro- or nanoscale VO_2 (M) particles. This method offers advantages such as large-scale synthesis and precise phase control, which are influenced by parameters like synthesis temperature, duration, precursor molar ratio, and concentration [12, 21, 27]. Temperature and reaction time are the most commonly studied parameters for VO_2 (M) synthesis, and increasing the reaction temperature or prolonging the reaction time results in higher content VO_2 (M) [12, 28, 29]. Additionally, dopants such as tungsten (W^{6+}) and molybdenum (Mo^{6+}), which are often used to modulate the T_c of VO_2 (M) to the targeted temperature [29-32] (for example W^{6+}, decreasing the T_c by approximately 23°C per atomic percent of dopant [1, 33]), are also reported to promote the formation of the VO_2 (M) phase (dopant-contained) [34].

Research by Ji et al. and Sirvent et al. [21, 28] has shown that pressure also has an enhancing effect on the transformation to VO_2 (M) without dopants, as demonstrated through hydrothermal experiments at 270 °C with varying filling ratios. The differences in pressure in these experiments were attributed to varying amounts of water vapor and carbon dioxide (CO_2) generated during the reaction. It is worth noting that the different pressure conditions were achieved only by changing the original filling ratio. The result obtained by Ji et al. [28] indicated that an increase in synthesis pressure from 64.5 bar to 73 bar resulted in a clear change in phase composition from a mixed composition of VO_2 (A) and VO_2 (M) phases to a single-phase composition of VO_2 (M). This result suggests that increased pressure might be an alternative favorable synthesis parameter to high temperature, and increased pressure could be relatively low-cost due to its one-step character in contrast to continuous heating. Both cited studies only investigated undoped VO_2 (M) synthesis, and their result may not be applicable to doped VO_2, which is applied in thermochromic windows for buildings, cars, etc. Hence, synthesis of dopant-modified VO_2 (M) under high pressure (i.e. 50-80 bar) at relatively mild temperature (i.e. <240 °C) and for relatively short duration (i.e. 24 h) seems a promising approach to reduce the energy cost for scalable VO_2 (M) synthesis.

In this work, we investigated the effect of externally introduced pressure on the formation of $V_{0.98}W_{0.02}O_2$ (M) using vanadium pentoxide (V_2O_5) and oxalic acid ($H_2C_2O_4 \cdot 2H_2O$) reactants with tungstic acid (H_2WO_4, the atomic percentage of W was 2.0 at%, which was a commonly used amount to modify the T_c to near to room temperature) via the hydrothermal synthesis method. Different pressures were applied by introducing nitrogen (N_2) or carbon

dioxide (CO_2) gas into the reactor before the reaction. Nitrogen is a commonly-used inert gas that does not react with VO_2, and the introduced specific amount of N_2 can be used as the only variable to control the pressure in the reactor to observe the possible independent influence of pressure to the phase components without other interfering factors. CO_2 is auto-produced during the hydrothermal synthesis reaction, and this gas was chosen in a second experimental series where the pressure in the reactor was adjusted via the introduction of specific amounts of CO_2. X-ray diffraction (XRD) and Differential Scanning Calorimetry (DSC) were employed to identify different VO_2 phases, and scanning electron microscopy (SEM) was used to examine the sample morphologies. This study aims to provide valuable insights into the parameter selection for synthesizing $V_{1-x}W_xO_2$ (M) via a hydrothermal method, exploring possible milder synthesis conditions (i.e. lower synthesis temperature) via increased pressure, potentially facilitating more efficient and scalable production.

2. Experimental Section

2.1 Materials

Oxalic acid dihydrate ($H_2C_2O_4 \cdot 2H_2O$, for synthesis) was purchased from Supelco® Analytical Products (Merck KGaA, Germany). Vanadium pentoxide (V_2O_5, 99.6%) and tungstic acid (H_2WO_4) were obtained from Thermo Fisher (Kandel, Germany). All chemical reagents in our experiments were used without further purification. Ultrapure water (MQ, 18.2 MΩ·cm, 25 °C) was obtained by purification of deionized water with a Merck system and used as the reaction solvent.

2.2 Preparation of $V_{0.98}W_{0.02}O_2$ particles via hydrothermal synthesis

In a typical procedure, 1.576 g $H_2C_2O_4 \cdot 2H_2O$ (0.25 M) were dissolved in 50 ml ultrapure water (18.2 $M\Omega \cdot cm^{-1}$ at 25 °C). 1.137g V_2O_5 (V_2O_5:$H_2C_2O_4 \cdot 2H_2O$=1:2 in molar ratio), 0.063g H_2WO_4 (the added atomic percent of W is 2 at%), and dissolved oxalic acid aqueous solution showing a bright orange color was added into the Teflon liner (~84 ml, the filling ratio is 60%) and the liner was put into a stainless-steel vessel (100 ml). The whole vessel was then put on a hotplate stirrer and surrounded by a heating mantle controlled by a temperature controller. After stirring at a speed of 1000 rpm at room temperature for 30 min, the resultant aqueous solution turned from orange to blue in color, and then the reactor was flushed 3 times with N_2 or CO_2 gas. By flushing, the air in the reactor was completely replaced by either N_2 or CO_2 gas, depending on the experiment type. Finally, the gas was introduced in the reactor to the desired pressure (0, 5, 10, 15 bar), and denoted as V_x (For N_2 gas, denoted as V_x, for CO_2 gas, denoted as $V_{x\text{-}CO2}$, with x = 0, 5, 10 and 15 bar; The initial pressure state of V_0 and $V_{0\text{-}CO2}$ were obtained by flushing the reactor with N_2 or CO_2, respectively, to replace air). The preset pressure was indicated by the pressure meter of the reactor. Then, the temperature was set to 235 or 240 °C (depending on the experiment) and a reaction duration of 24h was taken. The stirring speed was kept at 1000 rpm during the whole synthesis process. After 24 hours, the temperature was set to 40 °C and the solution was left to cool down. The obtained dark solution was centrifuged and washed twice using ultrapure water and once with ethanol, and then placed in an oven for drying overnight at 60 °C, obtaining the resultant dark particles.

2.3 Temperature setting information

To explore the potentially positive effect of pressure, we controlled the synthesis temperature at a milder temperature condition, 235 ºC, firstly, slightly lower than the reported lowest synthesis temperature (240-280 ºC) for the pure $V_{0.98}W_{0.02}O_2$ (M) phase in one step without subsequent annealing treatment. It should be noted that due to possible temperature fluctuation, equipment and reading error, the practical synthesis temperature might not be stable at 235 ºC during the whole synthesis with s fluctuation of 1-2 ºC. Samples synthesized at the temperature of 240 ºC were denoted V_{H-x}, with x = 0, 5, or 10 bar.

2.4 Characterizations

The crystal phase data of the $V_{0.98}W_{0.02}O_2$ nanoparticles were obtained by X-ray diffraction (XRD), performed on Bruker D2 Phaser (Bruker, Germany) with Cu tube source (λ = 0.154 nm) over the 2-theta range of 10°-70° and a scan speed of 0.500 s/step. The XRD peaks were searched and matched with the standard PDF cards using Highscore Plus software. The phase change temperature (τ_c) was detected by differential scanning calorimetry (DSC2A-02398, TA Instruments, US) with a scan rate of 10 °C/min under an N_2 environment from 20-350 ºC. The morphology of the particles was observed by scanning electron microscopy (SEM) using a Philips XL 30 FEG at an accelerating voltage of 10 kV (Philips, Netherlands). All samples were sputtered with a thin layer of gold before observation.

3. Results and Discussion

3.1 Synthesis of $V_{0.98}W_{0.02}O_2$ (M) at 235 ºC under different N_2 pressure

The temperature for synthesizing pure VO_2 (M) from V_2O_5 and $H_2C_2O_4$ reactants via hydrothermal synthesis is reported to be between 240-270 ºC [21]. To explore the lower

temperature boundary for synthesis, we selected a slightly lower temperature, 235 °C, as synthesis temperature. During the reaction, a probe was inserted into the reactor to record the real-time temperature, while the pressure meter on the high temperature-high pressure reactor monitored the internal pressure (Figure S1). The temperature and pressure data for all samples are presented in Table 1.

Table 1. Hydrothermal synthesis conditions of all samples.

Samples	Probe T[a] (°C)	Added gas	Added gas P[b] (bar)	Max. P (bar)
V_0	235	N_2	0	49
V_5	235	N_2	5	55
V_{10}	235	N_2	10	62
V_{15}	235	N_2	15	72
$V_{0\text{-}CO2}$	235	CO_2	0	46
$V_{5\text{-}CO2}$	235	CO_2	5	50
$V_{10\text{-}CO2}$	235	CO_2	10	58
$V_{15\text{-}CO2}$	235	CO_2	15	64
$V_{H\text{-}10\text{-}CO2}$	240	CO_2	10	69
$V_{H\text{-}0}$	240	N_2	0	53
$V_{H\text{-}5}$	240	N_2	5	56
$V_{H\text{-}10}$	240	N_2	10	67

[a] Temperature. [b] Pressure.

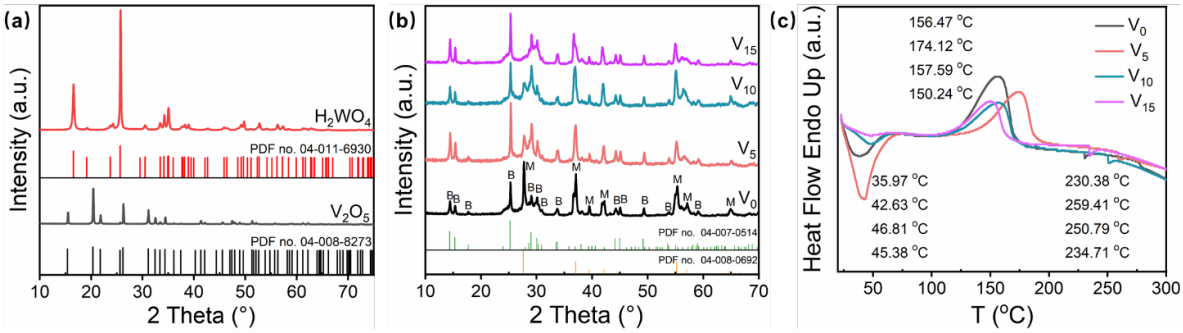

Figure 1. (a) XRD patterns of as-received V_2O_5 and H_2WO_4. (b) XRD patterns and (c) DSC results of V_0, V_5, V_{10}, and V_{15} synthesized at 235 °C under added N_2 pressure of 0, 5, 10, and 15 bar, respectively. The PDF no. of V_2O_5, H_2WO_4, VO_2 (B) and VO_2 (M) are 04-08-8273, 04-011-6930, 04-007-0514 and 04-008-0692, respectively.

XRD tests on V_2O_5 and H_2WO_4 were conducted first (Figure 1a). The characteristic peak of V_2O_5 at 20.4° and characteristic peak of H_2WO_4 at 25.7° are not observed in the pattern of obtained VO_2 (Figure 1b), indicating that V_2O_5 and H_2WO_4 reacted completely during the hydrothermal synthesis (V_2O_5:$H_2C_2O_4 \cdot 2H_2O$=1:2 in molar ratio and the added atomic percent of W is 2 at%). The crystal phases of the obtained samples were characterized by XRD (Figure 1b). According to the PDF standard of VO_2 (B) (04-007-0514) and VO_2 (M) (04-008-0692), in the V_0 sample, VO_2 (B) and $V_{0.98}W_{0.02}O_2$ (M) phases were identified, with two minor peaks for VO_2 (A) at the 2 theta of 47.2° and 47.7° (for simplicity, the W was not indicated in VO_2 (A), VO_2 (B) and VO_2 (D) phases). Increasing the N_2 gas pressure did not result in significant phase differences among the V_5, V_{10} and V_{15} samples, with VO_2 (B) and $V_{0.98}W_{0.02}O_2$ (M) phases present in all samples. Considering that the maximum pressure of the reactor was 100 bar, we did not increase the pressure further. The starting pressure results in a maximum pressure of 55, 62, and 72 bar in the vessel, respectively, at the reaction

temperature for V_5, $V_{10,}$ and V_{15} samples, with corresponding pressure differences of 6, 13, and 23 bar compared to V_0. Based on XRD results (Figure 1a) both VO_2 (B) and $V_{0.98}W_{0.02}O_2$ (M) phases were detected in all samples, without any obvious differences for increased pressure. In the reported experimental results by Ji et al. [28], pressure showed a positive effect on promoting the formation of VO_2 (M) when the maximum pressure increased from 64.5 bar to 73 bar in the reactor at 270 °C (the difference was 8.5 bar, undoped system), whereas a higher pressure change (23 bar) in our experiments did not show an influence of pressure on the reaction product, indicating pressure may not be a factor favoring the transformation to $V_{0.98}W_{0.02}O_2$ (M) phase. Due to the very high similarity of XRD peaks among VO_2 (A), VO_2 (D) and $V_{0.98}W_{0.02}O_2$ (M), VO_2 (A) and VO_2 (D) may not be identified unequivocally based on XRD data [12, 35-37].

To further verify the composition of our samples, DSC analysis was conducted to observe possible phase change peaks since DSC is known for its high sensitivity to crystal phases even for small content of a certain phase in analysed samples (Figure 1c). The phase transition endothermic peak between 30-50 °C corresponds to the transformation of $V_{0.98}W_{0.02}O_2$ (M) into $V_{0.98}W_{0.02}O_2$ (R). Additional peaks between 150-180 °C and 230-260 °C indicate the presence of VO_2 (A) and VO_2 (D), respectively[9, 38-40]. The transition temperature of VO_2 (B) is higher than 400 ºC, hence it was not observed in the DSC analysis. The DSC results confirmed that VO_2 (A) and VO_2 (D) were present in all four samples. Based on the phase evolution interpretation [41], VO_2 (M) can transform from VO_2 (A) and originally from VO_2

(B). VO_2 (D) has also been highlighted as an easier conversion path due to its structural similarity to VO_2 (M) [9]. Therefore, under these synthesis conditions, other phases including VO_2 (A), VO_2 (B), and VO_2 (D) had not completely transformed into $V_{0.98}W_{0.02}O_2$ (M) phase. These findings indicate that externally introduced N_2 pressure did not significantly affect the transformation to $V_{0.98}W_{0.02}O_2$ (M).

The X-ray diffraction (XRD) data of the first test samples (Figure 1a) and replicates (Figure S2) indicate that the characteristic peak intensity of the $V_{1-x}W_xO_2$ (M) phase at ~27.8° does not show a specific trend with N_2 pressure when all samples are considered (Figure S2a and S2b). For example, the characteristic peak intensity of $V_{0.98}W_{0.02}O_2$ (M) phase at ~27.8° seems to increase from $V_{0'}$ to $V_{5'}$, then decrease for $V_{10'}$ and then increase again for $V_{15'}$ (Figure S2a). This peak is prominent in V_0 but very low in $V_{0''}$. The DSC results (Figure S2b and Table S1) indicate that the phase transition enthalpy values (ΔH_m) for $V_{0'}$, $V_{5'}$, $V_{10'}$ and $V_{15'}$ are 1.57, 2.38, 5.09 and 0.81, respectively (Figure S2c and Table S1), and there is no clear trend with increased N_2 pressure. Hence, these findings suggest some variations that might be attributed to very slight temperature fluctuations in the heating system of the synthesis reactor. Our study highlights the pronounced sensitivity of phase composition to minor temperature variations (<5 °C), where even such small fluctuations can lead to noticeable differences in the relative proportions of resulting phases. Moreover, the synthesis duration may play a critical role, as phase transformations might still be occurring beyond 24 hours synthesis reaction time. Extending the synthesis time could potentially mitigate the variations in relative proportions of phases and promote more consistent phase formation.

However, focusing on the role of pressure, we can conclude that external introduced N_2 pressure did not exhibit a clearly positive or negative effect on the transformation of VO_2 (M) for the 24-hour reaction period.

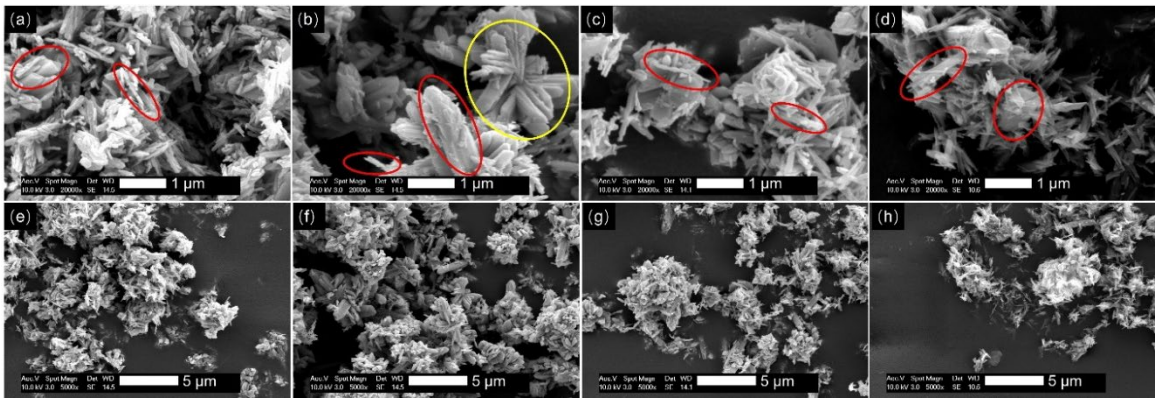

Figure 2. SEM microphotographs of (a) V_0, (b) V_5, (c) V_{10} and (d) V_{10}. Panels e, f, g and h are zoomed-out images of a, b, c and d, respectively (red circle indicated the needles and rods particles and yellow circle indicated the particle that have a trend to form "snowflake" shape).

SEM was utilized to characterize the particle morphology of V_0, V_5, V_{10} and V_{15} samples (Figure 2). The SEM microphotographs of V_0 (Figures 2a and 2e) revealed a mix of needles and rods (indicated by red circles), corresponding to VO_2 (B) or VO_2 (A). However, the characteristic "snowflake-shaped" particles of $V_{0.98}W_{0.02}O_2$ (M) [28, 41] were not observed. Similar observations were made for V_5 (Figures 2b and 2f), V_{10} (Figures 2c and 2g) and V_{15} (Figures 2d and 2h), where uneven needles and rods were present, but no definitive "snowflake-shaped" $V_{0.98}W_{0.02}O_2$ (M) particles were detected. Some rods appeared to be stacked together, suggesting a trend toward forming "snowflakes," but the process was still incomplete (Figure 2b, indicated by yellow circles). These SEM results were consistent with the XRD and DSC findings, indicating that the transformation from VO_2 (B) to $V_{0.98}W_{0.02}O_2$

(M) was not complete and that pressure did not significantly promote this transformation process. Therefore, the synthesis of $V_{0.98}W_{0.02}O_2$ (M) particles via hydrothermal methods under different N_2 pressures at 235 °C did not significantly alter the phase composition or morphology of the reaction product.

3.2 Synthesis of $V_{0.98}W_{0.02}O_2$ (M) at 235 under different CO_2 pressure

Previous studies have suggested that pressure facilitates the transformation to VO_2 (M) [21, 28]. In those studies, pressure differences were achieved by altering the reactor filling ratio, and consequently, the amount of CO_2 gas generated during the reaction of V_2O_5 and $H_2C_2O_4$ changed. This observation led us to investigate the effect of adding different amounts of CO_2 gas into the reactor, different from our previously mentioned experiments using N_2 gas.

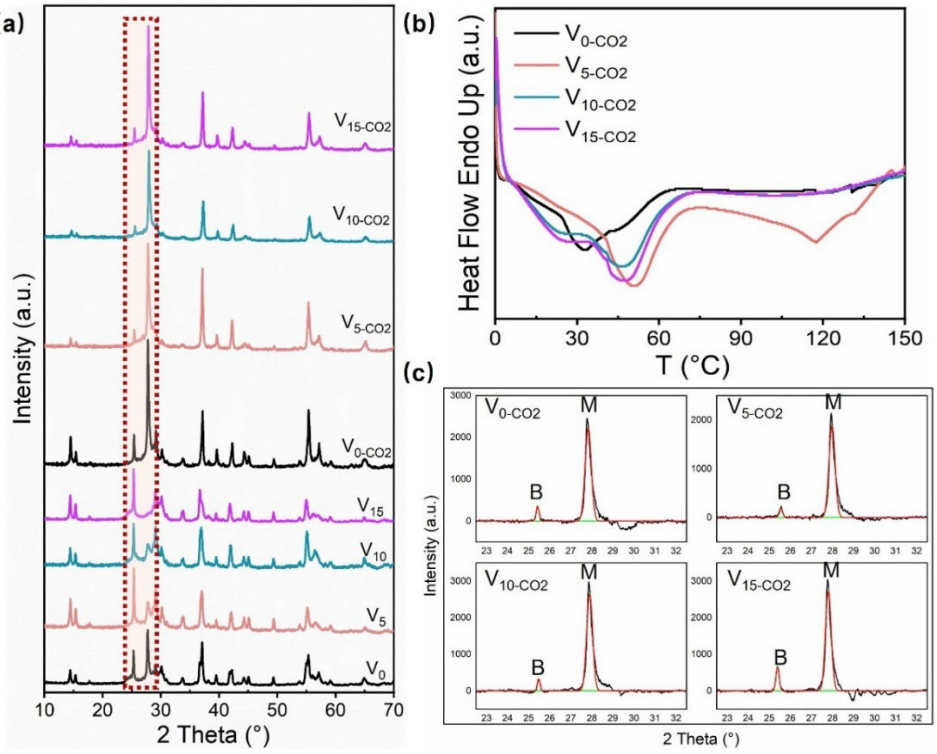

Figure 3. (a) XRD patterns of V_0, V_5, V_{10}, V_{15}, $V_{0\text{-}CO2}$, $V_{5\text{-}CO2}$, $V_{10\text{-}CO2}$ and $V_{15\text{-}CO2}$. (b) DSC results and (c) peak fitting curves of $V_{0\text{-}CO2}$, $V_{5\text{-}CO2}$, $V_{10\text{-}CO2}$ and $V_{15\text{-}CO2}$.

The XRD data of all samples synthesized at 235 ºC under 0, 5, 10 and 15 bar added CO_2 pressure (denoted as $V_{0\text{-}CO2}$, $V_{5\text{-}CO2}$, $V_{10\text{-}CO2}$ and $V_{15\text{-}CO2}$) are shown in Figure 3a. For comparison, the XRD data for samples synthesized at 235°C under N_2 gas (shown in Figure 1a) are also included in Figure 3a. A clear difference is observed: all the samples $V_{0\text{-}CO2}$, $V_{5\text{-}CO2}$, $V_{10\text{-}CO2}$ and $V_{15\text{-}CO2}$ exhibit a notable increase in the peak intensity of the $V_{1\text{-}x}W_xO_2$ (M) phase (~27.8°), coupled with a decrease in the peak intensity of the VO_2 (B) phase (~25.4°) compared with samples obtained under N_2 atmosphere (V_0, V_5, V_{10} and V_{15}). This indicates that a greater proportion of the VO_2 (B) phase was transformed into the $V_{1\text{-}x}W_xO_2$ (M) phase, which further grew into larger crystals (highlighted in the red dotted box in Figure 3a).

Table 2. Phase transition enthalpy of $V_{0.98}W_{0.02}O_2$ (M) synthesized at 235 ºC under 0, 5, 10, and 15 bar added CO_2 pressure.

Samples	$V_{0\text{-}CO2}$	$V_{5\text{-}CO2}$	$V_{10\text{-}CO2}$	$V_{15\text{-}CO2}$
ΔH_m (J/g) of $V_{0.98}W_{0.02}O_2$ (M)	7.66	9.77	12.02	14.37
Peak area percentage of $V_{0.98}W_{0.02}O_2$ (M)	88.1	93.0	94.4	94.7
pH of solutions after synthesis	3.37	3.17	3.02	2.98

The DSC results of the $V_{1-x}W_xO_2$ (M) phase for $V_{0\text{-}CO2}$, $V_{5\text{-}CO2}$, $V_{10\text{-}CO2}$ and $V_{15\text{-}CO2}$ (Figure 3b) and the detailed enthalpy values for $V_{1\text{-}x}W_xO_2$ (M) phase (Table 2) show that the phase transition enthalpy for these CO_2-treated samples increased significantly compared to their N_2 counterparts ($V_{0'}$, $V_{5'}$, $V_{10'}$, and $V_{15'}$). This suggests greater and more complete formation of $V_{1-x}W_xO_2$ (M) crystals, consistent with the XRD results.

In order to more clearly observe the relative content changes of VO_2 (B) and $V_{1-x}W_xO_2$ (M) phases under CO_2 gas, we selected the peaks at 25.4° and 27.8° as the characteristic peaks of VO_2 (B) and $V_{1-x}W_xO_2$ (M), respectively, and further carried out peak fitting and calculation of peak area for $V_{0\text{-}CO2}$, $V_{5\text{-}CO2}$, $V_{10\text{-}CO2}$ and $V_{15\text{-}CO2}$ using the *Origin* software (Figure 3c). Based on the peak areas, we conducted a semi-quantitative analysis of the phase content, with the percentage of the $V_{1-x}W_xO_2$ (M) phase recorded in Table 2. All CO_2-treated samples exhibit a lower peak intensity for the VO_2 (B) phase and a higher peak intensity for the $V_{1-x}W_xO_2$ (M) phase, with the peak area percentage of $V_{1-x}W_xO_2$ (M) ranging from 88% to 95%. compared to 30–60% for those synthesized under N_2 atmosphere ($V_{0'}$, $V_{5'}$, $V_{10'}$, and $V_{15'}$, Figure S3 and Table S2). Notably, the characteristic peak intensity and peak area percentage for $V_{0\text{-}CO2}$ were higher than those of any sample synthesized under N_2 gas. This observation may be attributed to the increased CO_2 introduction into the reactor, leading to the formation of carbonic acid (H_2CO_3) and the subsequent ionization of hydrogen ions (H^+) in water. These changes likely influenced the reduction-oxidation reaction between V_2O_5 and $H_2C_2O_4 \cdot 2H_2O$, which can be represented by the following equation:

$$V_2O_5\ (s) + H_2C_2O_4\ (s) \rightarrow 2VO_2\ (s) + H_2O\ (l) + 2CO_2\ (g)$$

The increase in acid concentration could shift the reaction equilibrium to the right, promoting the formation of VO_2. Furthermore, when comparing the final pressures of samples pre-filled with the same amount of N_2 and CO_2 (Table 1), such as V_0 and $V_{0\text{-}CO2}$, V_5 and $V_{5\text{-}CO2}$, V_{10} and $V_{10\text{-}CO2}$, and V_{15} and $V_{15\text{-}CO2}$, we observed that the final pressure in the CO_2 atmosphere was always lower than that in the N_2 atmosphere. Additionally, we observed that the peak area

percentage of $V_{1-x}W_xO_2$ (M) slightly increased with rising pressure, while the pH of the final solution after synthesis decreased marginally (Table 2). This could be due to the increased dissolution of CO_2 in water under higher pressure, leading to a greater concentration of H^+. However, as pressure continued to increase, the rate of pH decrease and the corresponding increase in the peak area percentage of $V_{1-x}W_xO_2$ (M) slowed (Table 2). This phenomenon may be due to the reversible nature of CO_2 dissolution in water, where the generation of H_2CO_3 leads to a subsequent reverse ionization of CO_2.

The addition of H^+ ions can indeed drive the reaction to the right, promoting the formation of VO_2. Previous studies have used H_2SO_4 (which produces H^+ ions in water) as a morphology control agent in the hydrothermal synthesis of VO_2, demonstrating that pH influence the phase structure of VO_2 [42-44]. Therefore, the effect of CO_2 on the transformation of $V_{1-x}W_xO_2$ (M) might be attributed to the dissolution of CO_2 in water, forming H_2CO_3 and subsequently ionizing H^+.

Although the relative content of VO_2 (B) phase decreased slightly and $V_{1-x}W_xO_2$ (M) phase increased under CO_2 atmosphere compared to N_2 gas, the VO_2 (B) phase remained detectable in all samples. This might be due to the limited solubility of H_2CO_3 in water, preventing a linear increase in H^+ concentration with increasing CO_2 pressure.

By comparing the samples synthesized under N_2 and CO_2 gas, we propose that the primary reason for the effect of pressure on the transformation of $V_{1-x}W_xO_2$ (M) is related to pressure-induced changes in CO_2 dissolution in water, which produces H^+ ions in the system. However, under the conditions of our experiments, the VO_2 (B) phase did not fully transform into

$V_{1-x}W_xO_2$ (M), likely due to the limited solubility of CO_2 in water.

Compared with Ji et al.'s work, the difference with our work can result from two aspects: 1) Hydrothermal temperature. Based on the Gibbs free energy formula,

$$\Delta G = \Delta U + p\Delta V - T\Delta S$$

When VO_2 (B) or VO_2 (A) spontaneously transforms into VO_2 (R), ΔG must be negative. According to literature [43], at a higher temperature, the transformation from VO_2 (B) to VO_2 (A) and finally to VO_2 (M) can be achieved, but this is not the case at lower temperature. Therefore, at higher temperature, ΔG is expected to be negative, indicating the absolute value of $-T\Delta S$ (+) is smaller than the absolute value of $p\Delta V$ (-). Concurrently, ΔG is expected to be positive at lower temperature, indicating the absolute value of $-T\Delta S$ (+) is larger than the absolute value of $p\Delta V$ (-). Therefore, decreasing temperature will lead to a larger decrease in the absolute value of $p\Delta V$ (-) compared to $-T\Delta S$ (+), and thus the transformation from VO_2 (B) to VO_2 (A) and finally to VO_2 (M) is less likely to occur spontaneously. Ji et al. conducted their experiments at 270 °C, whereas our experiments were performed at 235 °C and 240 °C. This temperature difference may explain why we did not observe pressure-promoted phase transitions. 2) Dopant. Another difference lies in the fact that Ji et al. obtained VO_2 (A) phase at 270 ºC without dopant, whereas in all our reactions with 2 at.% tungsten dopant at 240 ºC, VO_2 (A) was not detected in the XRD results. This might be attributed to the reason that VO_2 (A) is a metastable phase, and it becomes less stable with tungstic acid as dopant [45]. As a result, no transformation from the metastable VO_2 (A) phase to VO_2 (R) is observed based on XRD results. However, VO_2 (A) was still detected in DSC, probably because VO_2 (A) was

not completely transformed to VO_2 (R) at our relative low synthesis temperature (240 °C), and a very small content of VO_2 (A) might be present and be detected by the highly sensitive DSC device. Considering practical applications, such as smart windows, where VO_2 is frequently used, reducing the intrinsic phase transition temperature of VO_2 by adding dopants, such as tungsten, is essential. Therefore, studying the synthesis parameters of tungsten-doped VO_2 systems is of significant importance.

Synthesis of $V_{0.98}W_{0.02}O_2$ (M) at 235 and 240 °C under CO_2 pressure of 10 bar

The XRD result for the sample obtained under 10 bar CO_2 pressure at 235 °C ($V_{10\text{-}CO2}$) is shown in Figure 4a. The VO_2 (B) phase was still present, and uneven needles and rods were also determined in the SEM microphotographs (Figure S4a and 4c). The maximum pressure tested for $V_{10\text{-}CO2}$ (58 bar) was lower than V_{10} (N_2, 62 bar), which might be because some CO_2 gas dissolved in the solution. On this basis, we then slightly increased the synthesis temperature to 240 °C and marked the obtained sample synthesized at 240 °C and under 10 bar CO_2 as $V_{H\text{-}10\text{-}CO2}$. The practical temperature and pressure are recorded in Table 1. Only $V_{0.98}W_{0.02}O_2$ (M) phase peaks appear in the XRD pattern of this sample (Figure 4a), thus lacking VO_2 (B) peaks. Additionally, the characteristic peaks for $V_{0.98}W_{0.02}O_2$ (M) reached a higher intensity, indicating that the crystals were larger and the transformation to $V_{0.98}W_{0.02}O_2$ (M) was more complete at this higher temperature. The SEM microphotographs of $V_{H\text{-}10\text{-}CO2}$ also indicated the large and complete "snow-flakes" $V_{0.98}W_{0.02}O_2$ (M) formed (Figure S4b and 4d).

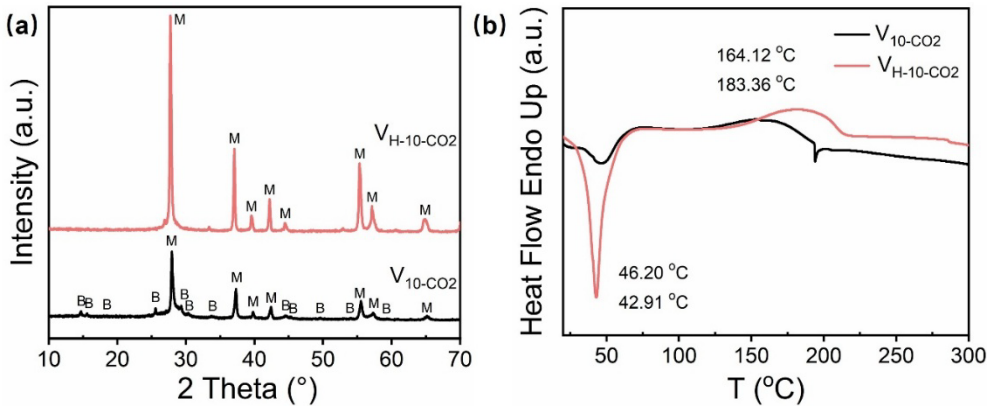

Figure 4. (a) XRD patterns and (b) DSC results of $V_{10\text{-}CO2}$ and $V_{H\text{-}10\text{-}CO2}$ at 235 °C and 240 °C, respectively, under added CO_2 pressure of 10 bar.

The DSC comparison of $V_{10\text{-}CO2}$ and $V_{H\text{-}10\text{-}CO2}$ was shown in Figure 4b. Both samples displayed peaks for $V_{0.98}W_{0.02}O_2$ (M) at 40-50 °C and VO_2 (A) at 160-190 °C, but $V_{H\text{-}10\text{-}CO2}$ exhibited a sharper peak and a higher phase transition enthalpy (23.25 J/g) compared to $V_{10\text{-}CO2}$ (10.86 J/g), indicating larger $V_{0.98}W_{0.02}O_2$ (M) crystals. Both the XRD and DSC results suggest that the transformation to $V_{0.98}W_{0.02}O_2$ (M) is more complete at the higher temperature. However, with the increase in temperature, the maximum pressure increased correspondingly from 58 to 69 bar. Therefore, it is challenging to unambiguously conclude whether the pressure played a critical role in the transformation to $V_{0.98}W_{0.02}O_2$ (M).

In summary, it seems that temperature plays a crucial role in the phase transformation to $V_{0.98}W_{0.02}O_2$ (M) by comparing $V_{10\text{-}CO2}$ and $V_{H\text{-}10\text{-}CO2}$ (introducing the same amount of CO_2), while externally introduced pressure has limited significant effect. Higher synthesis temperatures lead to a more complete transformation and the formation of larger $V_{0.98}W_{0.02}O_2$ (M) crystals. This might be attributed to the reason the increase in temperature provided the energy to transform from VO_2 (A) or VO_2 (B) phases to $V_{0.98}W_{0.02}O_2$ (M) phase.

3.3 Synthesis of $V_{0.98}W_{0.02}O_2$ (M) at 240 °C under different N_2 pressure

To evaluate the potential effects of externally introduced pressure on transformation to $V_{0.98}W_{0.02}O_2$ (M) at the synthesis temperature of 240 °C, a series of samples (V_{H-0}, V_{H-5}, and V_{H-10}) were synthesized under varying N_2 pressures, and the recorded synthesis parameters are shown in Table 1. The XRD results in Figure 5a revealed that the spectra of these three samples are nearly identical, all displaying the $V_{0.98}W_{0.02}O_2$ (M) phase with similar peak intensities, and VO_2 (A) and VO_2 (B) phases were not detected. The possible reason could be that all VO_2 (A) and VO_2 (B) phases have transformed into $V_{0.98}W_{0.02}O_2$ (M) phase, or only a tiny amount of VO_2 (A) or VO_2 (B) remained, which was not detected by the XRD equipment.

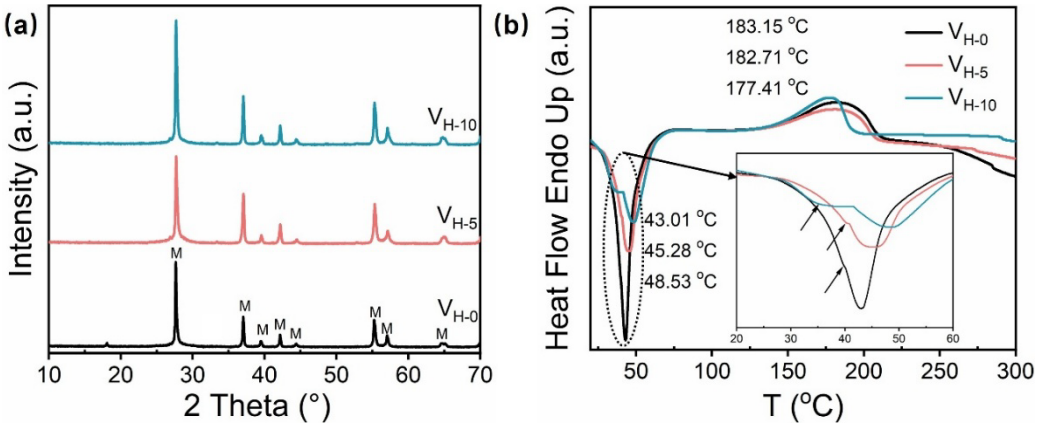

Figure 5. (a) XRD patterns and (b) DSC results of V_{H-0}, V_{H-5} and V_{H-10}, respectively, under added N_2 pressure of 0, 5, and 10 bar.

The DSC results of V_{H-0}, V_{H-5}, and V_{H-10} was analyzed using DSC (Figure 5b). Compared to samples synthesized at 235 °C, V_{H-0}, V_{H-5} and V_{H-10} exhibited a sharper endothermic peak around 45°C, corresponding to the transformation of $V_{0.98}W_{0.02}O_2$ (M) into $V_{0.98}W_{0.02}O_2$ (R).

This sharper peak indicated the $V_{0.98}W_{0.02}O_2$ (M) crystal was larger, and the transformation to $V_{0.98}W_{0.02}O_2$ (M) was more complete. We also observed a peak differentiating phenomenon in these three samples (the inset figure in Figure 5b), which indicated that multiple species of $V_{0.98}W_{0.02}O_2$ (M) were present in the product with different particle sizes and/or degree or distribution of doping[34]. Additionally, a phase transition at around 180°C, attributed to VO_2 (A), was observed in the DSC curves, indicating the presence of VO_2 (A) in the samples. We calculated the phase transition enthalpy and the enthalpy ratio of $V_{0.98}W_{0.02}O_2$ (M) and VO_2 (A) phases for these samples, as recorded in Table 3. With increasing synthesis temperature, the phase transition enthalpy of $V_{0.98}W_{0.02}O_2$ (M) and its ratio to VO_2 (A) significantly increased, demonstrating that temperature indeed has a promoting effect on the transformation from $V_{0.98}W_{0.02}O_2$ (M) to VO_2 (A). However, due to the low content of VO_2 (A), the transformation was not detected by XRD.

Table 3. Phase transition enthalpy of $V_{0.98}W_{0.02}O_2$ (M) and VO_2 (A) as well their ratio of all samples.

Samples		V_0	V_5	V_{10}	V_{15}	$V_{10\text{-}CO2}$	$V_{H\text{-}10\text{-}CO2}$	$V_{H\text{-}0}$	$V_{H\text{-}5}$	$V_{H\text{-}10}$
ΔH_m (J/g)	$V_{0.98}W_{0.02}O_2$ (M)	4.57	8.70	2.39	1.40	10.86	23.25	26.06	22.64	19.31
	VO_2 (A)	12.56	9.46	7.86	6.68	10.23	13.00	14.31	12.25	10.35
Ratio		0.36	0.92	0.30	0.21	1.06	1.79	1.82	1.85	1.87

The enthalpy ratio of $V_{0.98}W_{0.02}O_2$ (M) to VO_2 (A) phases increased with higher synthesis temperature, indicating that higher temperatures favor the transformation to the $V_{0.98}W_{0.02}O_2$

(M) phase. However, when comparing samples synthesized under the same temperature conditions, no positive effect of pressure on the transformation to $V_{0.98}W_{0.02}O_2$ (M) was observed. Comparing the synthesis temperature of samples $V_{H\text{-}0}$, $V_{H\text{-}5}$, and $V_{H\text{-}10}$ with samples V_0, V_5, V_{10} and V_{15}, it can be found that with a small temperature difference (5 °C, and the difference might even be smaller due to the temperature fluctuation), the phase composition could be totally different, indicating the high sensitivity of phase transformation to temperature. This conclusion highlights the significance of precise temperature control for synthesizing $V_{1-x}W_xO_2$ (M) via a hydrothermal method.

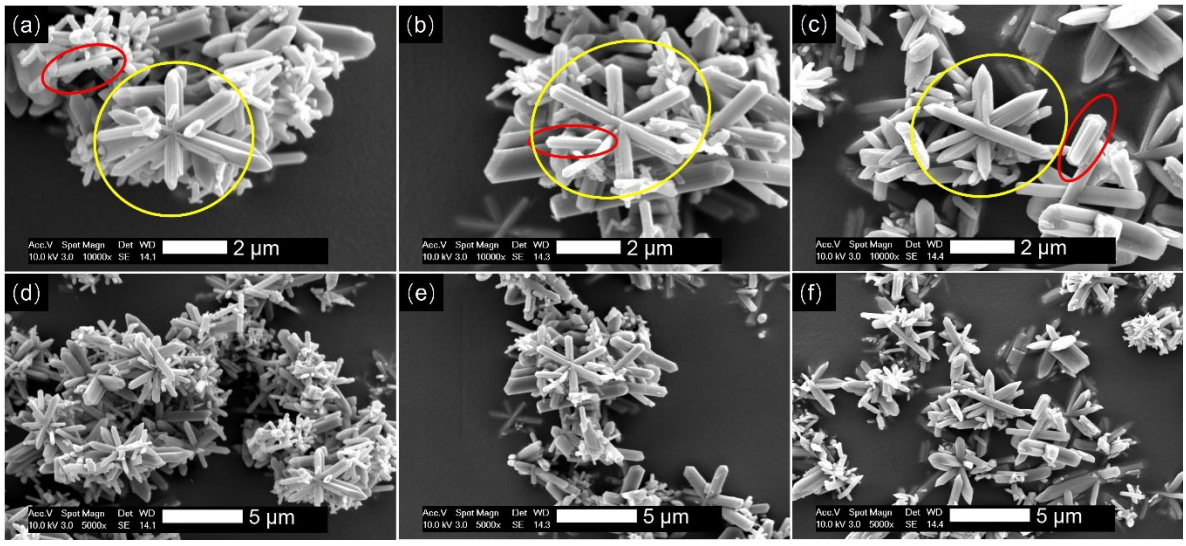

Figure 6. SEM microphotographs of (a) $V_{H\text{-}0}$, (b) $V_{H\text{-}5}$ and (c) $V_{H\text{-}10}$. Panels d, e and f are the zoomed-out images of a, b and c respectively (red circle indicated the rods particles and yellow circle indicated the complete "snowflake-shaped" particles).

The morphology of $V_{H\text{-}0}$, $V_{H\text{-}5}$, and $V_{H\text{-}10}$ samples, synthesized at a higher temperature, was observed by SEM (Figure 6). "Snowflake" structures (indicated by yellow circles), attributed to $V_{0.98}W_{0.02}O_2$ (M), were observed in all samples. Additionally, some single rods (indicated

by red circles) were also present in the samples. Based on the phase evolution interpretation and the DSC results, these rods are likely VO_2 (A) or VO_2 (B) that have not fully transformed into the $V_{0.98}W_{0.02}O_2$ (M) phase. Overall, there were no significant morphological differences among $V_{H\text{-}0}$, $V_{H\text{-}5}$, and $V_{H\text{-}10}$, further corroborating the XRD and DSC findings that suggest externally introduced pressure did not significantly affect the transformation to $V_{0.98}W_{0.02}O_2$ (M) under our employed synthesis conditions.

4. Conclusion

In summary, a series of $V_{0.98}W_{0.02}O_2$ (M) particles were synthesized under varying externally introduced pressure and temperature via a hydrothermal method, employing N_2 and CO_2 gases to adjust the synthesis pressure. XRD, DSC, and SEM analyses of the obtained samples revealed that externally introduced pressure has no direct significant effect on the formation of the $V_{0.98}W_{0.02}O_2$ (M) phase, whereas it may slightly affect the transformation of $V_{0.98}W_{0.02}O_2$ (M) by affecting the dissolution of CO_2 in water and then the H^+ content of the solution. Instead, the formation of the $V_{0.98}W_{0.02}O_2$ (M) phase was highly sensitive to the synthesis temperature with significant phase variations when the temperature difference was extremely small (<5 ^oC). This conclusion provides insight on the role of externally introduced pressure, unveiling the possible promoting effect of pressure on the dissolution of CO_2 and further indirect effect on the pH and phase components, highlighting the significance of precise temperature control on synthesizing $V_{1-x}W_xO_2$ (M) particles via a hydrothermal method. This work provides valuable suggestion for large-scale preparation of $V_{1-x}W_xO_2$ (M)

and promoting its application in smart windows for buildings, automotive glazing, and other energy-efficient technologies.

Declaration of interests

The authors declare that they have no known competing financial interests or personal relationships that could have appeared to influence the work reported in this paper.

Acknowledgements

We gratefully acknowledge Fonds Wetenschappelijk Onderzoek—Vlaanderen (FWO) for the fundamental senior research project (G0C0423N) which supports this study.

References

[1] M. Li, S. Magdassi, Y. Gao, Y. Long, Hydrothermal Synthesis of VO_2 Polymorphs: Advantages, Challenges and Prospects for the Application of Energy Efficient Smart Windows, Small 13 (2017) 1701147. https://doi.org/https://doi.org/10.1002/smll.201701147.

[2] Y. Zhang, X. Zhang, Y. Huang, C. Huang, F. Niu, C. Meng, X. Tan, One-step hydrothermal conversion of VO_2 (B) into W-doped VO_2 (M) and its phase transition and optical switching properties, Solid State Commun. 180 (2014) 24-27. https://doi.org/https://doi.org/10.1016/j.ssc.2013.10.028.

[3] D. Hagrman, J. Zubieta, C.J. Warren, L.M. Meyer, M.M.J. Treacy, R.C. Haushalter, A New Polymorph of VO_2 Prepared by Soft Chemical Methods, J. Solid State Chem. 138 (1998) 178-182. https://doi.org/https://doi.org/10.1006/jssc.1997.7575.

[4] Y. Luo, S. Chandrasekaran, B. Hu, R. Chen, M. Worsley, B. Dunn, Transforming nanoscale VO_2 (B) into a scalable sodium-ion electrode, Nano Res. 17 (2024) 8809-8818.

https://doi.org/10.1007/s12274-024-6688-0.

[5] W. Ling, Z. Zou, S. Zhang, X. Peng, S. Luo, X. Tang, J. Geng, Unique CO2-modified VO_2 (B) nanosheets for lithium batteries with high electrochemical performance, J. Alloys Compd. 936 (2023) 168215. https://doi.org/https://doi.org/10.1016/j.jallcom.2022.168215.

[6] F. Cui, J. Zhao, D. Zhang, Y. Fang, F. Hu, K. Zhu, VO_2 (B) nanobelts and reduced graphene oxides composites as cathode materials for low-cost rechargeable aqueous zinc ion batteries, Chem. Eng. J. 390 (2020) 124118. https://doi.org/https://doi.org/10.1016/j.cej.2020.124118.

[7] S. Lee, X.-G. Sun, A.A. Lubimtsev, X. Gao, P. Ganesh, T.Z. Ward, G. Eres, M.F. Chisholm, S. Dai, H.N. Lee, Persistent Electrochemical Performance in Epitaxial VO_2 (B), Nano Lett. 17 (2017) 2229-2233. https://doi.org/10.1021/acs.nanolett.6b04831.

[8] M.K. Shahzad, R.Z. Abbas Manj, G. Abbas, R.A. Laghari, S.S. Akhtar, M.A. Khan, M.B. Tahir, S. Znaidia, M. Alzaid, Influence of VO_2 based structures and smart coatings on weather resistance for boosting the thermochromic properties of smart window applications, RSC Adv. 12 (2022) 30985-31003. https://doi.org/10.1039/D2RA04661J.

[9] L. Liu, F. Cao, T. Yao, Y. Xu, M. Zhou, B. Qu, B. Pan, C. Wu, S. Wei, Y. Xie, New-phase VO_2 micro/nanostructures: investigation of phase transformation and magnetic property, New J. Chem. 36 (2012) 619-625. https://doi.org/10.1039/c1nj20798a.

[10] D. Wang, D. Guo, Z. Zhao, C. Ling, J. Li, S. Hong, Y. Zhao, H. Jin, Surface modification-assisted solvent annealing to prepare high quality M-phase VO_2 nanocrystals for flexible thermochromic films, Sol. Energy Mater. Sol. Cells 200 (2019) 110031.

https://doi.org/https://doi.org/10.1016/j.solmat.2019.110031.

[11] H.M. Barra, S.K. Chen, N. Tamchek, Z.A. Talib, O.J. Lee, K.B. Tan, Phase, Microstructure, Thermochromic, and Thermophysical Analyses of Hydrothermally Synthesized W-Doped VO_2 Nanopowder, Adv. Mater. Sci. Eng. 2021 (2021) 8582274. https://doi.org/https://doi.org/10.1155/2021/8582274.

[12] S. Wang, C. Li, S. Tian, B. Liu, X. Zhao, Facile synthesis of VO_2 (D) and its transformation to VO_2 (M) with enhanced thermochromic properties for smart windows, Ceram. Int. 2020, 46, 14739-14746 Ceram. Int. 46 (2020) 14739-14746. https://doi.org/https://doi.org/10.1016/j.ceramint.2020.02.278.

[13] M. Saini, B.S. Dehiya, A. Umar, VO_2 (M)@CeO_2 core-shell nanospheres for thermochromic smart windows and photocatalytic applications, Ceram. Int. 46 (2020) 986-995. https://doi.org/10.1016/j.ceramint.2019.09.062.

[14] L. Wu, M. Li, L. Li, S. Xu, F. Zou, G. Li, Spatially confined growth of VO_2 (M) nanoparticles with improved thermochromic property, Ceram. Int. 50 (2024) 11539-11547. https://doi.org/https://doi.org/10.1016/j.ceramint.2024.01.054.

[15] K. Li, M. Li, C. Xu, Y. Luo, G. Li, VO_2 (M) nanoparticles with controllable phase transition and high nanothermochromic performance, J. Alloys Compd. 816 (2020) 152655. https://doi.org/https://doi.org/10.1016/j.jallcom.2019.152655.

[16] J. Qi, D. Zhang, Q. He, L. Zeng, Y. Liu, Z. Wang, A. Zhong, X. Cai, F. Ye, P. Fan, Independent regulation of electrical properties of VO_2 for low threshold voltage electro-optic switch applications, Sens. Actuators A Phys. 335 (2022) 113394.

https://doi.org/https://doi.org/10.1016/j.sna.2022.113394.

[17] B. Li, Z. Wang, S. Zhao, C. Hu, L. Li, M. Liu, J. Zhu, T. Zhou, G. Zhang, J. Jiang, C. Zou, Enhanced Pd/a-WO_3/VO_2 Hydrogen Gas Sensor Based on VO_2 Phase Transition Layer, Small Methods 6 (2022) 2200931. https://doi.org/https://doi.org/10.1002/smtd.202200931.

[18] Y. Wang, Y. Hong, X. Hu, Y. Ye, P. Wang, J. Luo, A. Yin, Z. Ren, H. Liu, X. Qi, J. Liu, S. He, S. Yu, J. Wei, Flexible Fabric Temperature Sensor Based on VO_2/Pedot:Pss with High Performance, Adv. Mater. Technol. 8 (2023) 2300898. https://doi.org/https://doi.org/10.1002/admt.202300898.

[19] Y. Cui, Y. Ke, C. Liu, Z. Chen, N. Wang, L. Zhang, Y. Zhou, S. Wang, Y. Gao, Y. Long, Thermochromic VO_2 for Energy-Efficient Smart Windows, Joule 2 (2018) 1707-1746. https://doi.org/10.1016/j.joule.2018.06.018.

[20] S. Chen, Z.W. Wang, H. Ren, Y.L. Chen, W.S. Yan, C.M. Wang, B.W. Li, J. Jiang, C.W. Zou, Gate-Controlled VO_2 Phase Transition for High-Performance Smart Windows, Sci. Adv. 5 (2019) eaav6815. https://www.science.org/doi/10.1126/sciadv.aav6815.

[21] P. Sirvent, G. Pérez, A. Guerrero, Efficient VO_2 (M) synthesis to develop thermochromic cement-based materials for smart building envelopes, Mater. Chem. Phys. 269 (2021) 124765. https://doi.org/10.1016/j.matchemphys.2021.124765.

[22] G.P. Nagabhushana, G.T. Chandrappa, Facile solution combustion synthesis of monoclinic VO_2: a unique and versatile approach, J. Mater. Chem. A 1 (2013) 11539-11542. https://doi.org/10.1039/C3TA11692A.

[23] M. Li, C. Fang, Y. Cheng, X. Zhang, H. Han, J. Zhao, Y. Zhang, A facile pathway to

fabricate VO_2 (M) nanoparticles via sol-gel method for flexible thermochromic films with efficient infrared stealth, Vacuum 221 (2024) 112885. https://doi.org/10.1016/j.vacuum.2023.112885.

[24] Y. Li, F. Kong, B. Wang, Y. Zhao, Z. Wang, Preparation of shape-controlling VO_2 (M/R) nanoparticles via one-step hydrothermal synthesis, Front. Optoelectron. 14 (2021) 311-320. https://doi.org/10.1007/s12200-020-1006-2.

[25] L. Zhang, J. Yao, Y. Guo, F. Xia, Y. Cui, B. Liu, Y. Gao, VO_2 (A) nanorods: One-pot synthesis, formation mechanism and thermal transformation to VO_2 (M), Ceram. Int. 44 (2018) 19301-19306. https://doi.org/https://doi.org/10.1016/j.ceramint.2018.07.157.

[26] S.-i. Kwon, M. Hagiwara, S.-h. Kim, S. Fujihara, Multistep synthesis of VO_2 (M) nanoparticles and their application to thermochromic hybrid films for IR modulation, Int. J. Appl. Ceram. Technol. 2023, 20, 1997-2008 Int. J. Appl. Ceram. Technol. 20 (2023) 1997-2008. https://doi.org/https://doi.org/10.1111/ijac.14316.

[27] S. Ji, F. Zhang, P. Jin, Unexpected phase transformation from VO_2 (R) to VO_2 (A) during hydrothermal treatment in the V_2O_5–$H_2C_2O_4$–H_2O system, Chem. Intermed. 37 (2011) 493-502 Chem. Intermed. 2011, 37, 493-502. https://doi.org/10.1007/s11164-011-0290-2.

[28] S. Ji, F. Zhang, P. Jin, Selective formation of VO_2 (A) or VO_2 (R) polymorph by controlling the hydrothermal pressure, J. Solid State Chem. 184 (2011) 2285-2292. https://doi.org/https://doi.org/10.1016/j.jssc.2011.06.029.

[29] R. Chen, L. Miao, H. Cheng, E. Nishibori, C. Liu, T. Asaka, Y. Iwamoto, M. Takata, S. Tanemura, One-step hydrothermal synthesis of $V_{1-x}W_xO_2$ (M/R) nanorods with superior

doping efficiency and thermochromic properties, J. Mater. Chem. A 3 (2015) 3726-3738. https://doi.org/10.1039/C4TA05559D.

[30] Y. Zhang, J. Zhang, X. Zhang, Y. Deng, Y. Zhong, C. Huang, X. Liu, X. Liu, S. Mo, Influence of different additives on the synthesis of VO_2 polymorphs, Ceram. Int. 39 (2013) 8363-8376. https://doi.org/https://doi.org/10.1016/j.ceramint.2013.04.016.

[31] X. Tan, T. Yao, R. Long, Z. Sun, Y. Feng, H. Cheng, X. Yuan, W. Zhang, Q. Liu, C. Wu, Y. Xie, S. Wei, Unraveling Metal-insulator Transition Mechanism of VO_2 Triggered by Tungsten Doping, Sci. Rep. 2 (2012) 466. https://doi.org/10.1038/srep00466.

[32] N. Numan, I.G. Madiba, B.S. Khanyile, Z.M. Khumalo, M. Maaza, Hydrothermal synthesis and characterization of undoped and W-doped vanadium dioxide nanorods for thermochromic application, J. Cryst. Growth 590 (2022) 126702. https://doi.org/https://doi.org/10.1016/j.jcrysgro.2022.126702.

[33] Y. Zhou, S. Ji, Y. Li, Y. Gao, H. Luo, P. Jin, Microemulsion-based synthesis of $V_{1-x}W_xO_2$@SiO_2 core–shell structures for smart window applications, J. Mater. Chem. C 2 (2014) 3812-3819. https://doi.org/10.1039/C3TC32282C.

[34] K. Timmers, A. Chote, L. Leufkens, R. Habets, K. Elen, M.A. Verheijen, M.K. Van Bael, D. Mann, P. Buskens, Hydrothermal Synthesis of Monoclinic VO_2 Microparticles without Use of Hazardous Reagents: A Key Role for the W-Dopant, Inorg. Chem. 63 (2024) 5400-5413. https://doi.org/10.1021/acs.inorgchem.3c03999.

[35] S.S. Saeidi, B. Vaseghi, G. Rezaei, H. Khajehsharifi, D. Jenkins, Magnetic, optical and phase transformation properties of Fe and Co doped VO_2 (A) nanobelts, J. Solid State Chem.

306 (2022) 122729. https://doi.org/https://doi.org/10.1016/j.jssc.2021.122729.

[36] Y. Chen, Q. Ma, X. Li, M. Mudasar, X. Zhao, X. Cheng, J. Liu, Synthesis, characterization and electromagnetic absorbing performance of multi-step petaloid morphology VO_2 (M), Ceram. Int. 46 (2020) 25493-25502. https://doi.org/https://doi.org/10.1016/j.ceramint.2020.07.020.

[37] Y. Zhang, M. Fan, F. Niu, W. Wu, C. Huang, X. Liu, H. Li, X. Liu, Belt-like VO_2 (M) with a rectangular cross section: A new route to prepare, the phase transition and the optical switching properties, Curr. Appl. Phys. 12 (2012) 875-879. https://doi.org/https://doi.org/10.1016/j.cap.2011.11.024.

[38] M. Li, D.-B. Li, J. Pan, J.-C. Lin, G.-H. Li, Selective Synthesis of Vanadium Oxides and Investigation of the Thermochromic Properties of VO_2 by Infrared Spectroscopy, Eur. J. Inorg. Chem. 2013 (2013) 1207-1212. https://doi.org/https://doi.org/10.1002/ejic.201201118.

[39] Y. Zhang, X. Tan, C. Huang, C. Meng, Hydrothermal treatment with VO_2 (B) nanobelts for synthesis of VO_2 (A) and W doped VO_2 (M) nanobelts, Mater. Res. Innovations 19 (2015) 295-302. https://doi.org/10.1179/1433075X15Y.0000000001.

[40] J.C. Valmalette, J.R. Gavarri, High efficiency thermochromic VO_2 (R) resulting from the irreversible transformation of VO_2 (B), Mater. Sci. Eng. B 54 (1998) 168-173. https://doi.org/https://doi.org/10.1016/S0921-5107(98)00148-2.

[41] W. Yu, S. Li, C. Huang, Phase evolution and crystal growth of VO_2 nanostructures under hydrothermal reactions, RSC Adv. 6 (2016) 7113-7120. https://doi.org/10.1039/C5RA23898F.

[42] R. Shi, J. Wang, X. Cai, L. Zhang, P. Chen, S. Liu, L. Zhang, W. Ouyang, N. Wang, C. Cheng, Axial Modulation of Metal–Insulator Phase Transition of VO_2 Nanowires by Graded Doping Engineering for Optically Readable Thermometers, J. Phys. Chem. C, 121 (2017) 24877-24885. https://doi.org/10.1021/acs.jpcc.7b08946

[43] S. Ji, Y. Zhao, F. Zhang, P. Jin, Direct formation of single crystal VO_2(R) nanorods by one-step hydrothermal treatment, J. Cryst. Growth, 312 (2010) 282-286. https://doi.org/10.1016/j.jcrysgro.2009.10.026

[44] Y. Li, S. Ji, Y. Gao, H. Luo, M. Kanehira, Core-shell VO_2@TiO2 nanorods that combine thermochromic and photocatalytic properties for application as energy-saving smart coatings, Sci. Rep., 3 (2013) 1370. https://doi.org/10.1038/srep01370

[45] S. Ji, Y. Zhao, F. Zhang, P. Jin, Synthesis and phase transition behavior of w-doped VO_2 (A) nanorods, J. Ceram. Soc. Jpn., 118 (2010) 867-871. https://doi.org/10.2109/jcersj2.118.867